Electron paramagnetic resonance proof for the existence of molecular hydrino

Hagen, Wilfred R.; Mills, Randell L.

DOI
10.1016/j.ijhydene.2022.05.156

Publication date
2022

Document Version
Final published version

Published in
International Journal of Hydrogen Energy

Available online at www.sciencedirect.com

ScienceDirect

journal homepage: www.elsevier.com/locate/he

Electron paramagnetic resonance proof for the existence of molecular hydrino

Wilfred R. Hagen [a,**], *Randell L. Mills* [b,*]

[a] *Department of Biotechnology, Delft University of Technology, Delft, the Netherlands*
[b] *Brilliant Light Power Inc, Cranbury, NJ, USA*

HIGHLIGHTS

- New allotrope of molecular hydrogen recoded by EPR.
- New molecular orbital structure confirmed having a paired and an unpaired electron.
- SQUID behavior noted for a molecular orbital.
- New fastest gas migration velocity recorded by gas chromatography.
- New state of molecular hydrogen is the basis of a new power source.

GRAPHICAL ABSTRACT

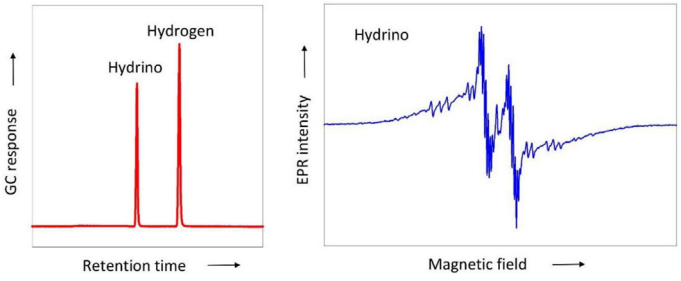

ARTICLE INFO

Article history:
Received 15 March 2022
Received in revised form
11 May 2022
Accepted 18 May 2022
Available online 11 June 2022

ABSTRACT

Quantum mechanics postulates that the hydrogen atom has a stable ground state from which it can be promoted to excited states by capture of electromagnetic radiation, with the energy of all possible states given by $E_n = -13.598/n^2$ eV, in which $n \geq 1$ is a positive integer. It has been previously proposed that the $n = 1$ state is not the true ground state, and that so-called hydrino states of lower energy can exist, which are characterized by fractional quantum numbers $n = 1/p$, in which $1 < p \leq 137$ is a limited integer. Electron transition to a hydrino state, H(1/p) is non-radiative and requires a quantized amount of energy, $2mE_1$ (m is an integer), to be transferred to a catalyst. Numerous putative hydrino-forming reactions have been previously explored and the products have been characterized by a range of analytical methods. Molecular hydrino has been predicted to be paramagnetic. Here, we give an account of an electron paramagnetic resonance (EPR) study of molecular hydrino $H_2(1/4)$ that was produced as gaseous inclusion in polymeric Ga(O)OH by a plasma reaction of atomic hydrogen with non-hydrogen bonded water as the catalyst. A sharp, complex, multi-line EPR spectrum is found, whose detailed properties prove to be consistent with predictions from hydrino theory. Molecular hydrino was also identified in gas chromatography as a compound faster than molecular hydrogen.

* *Corresponding author.*
** *Corresponding author.*
E-mail addresses: w.r.hagen@tudelft.nl (W.R. Hagen), rmills@brilliantlightpower.com (R.L. Mills).

https://doi.org/10.1016/j.ijhydene.2022.05.156

Introduction

The quantized energy levels of the hydrogen atom are $E_n = -13.598/n^2$ eV, in which the principal quantum number n is a positive integer. The electronic ground state has $n = 1$. Higher states can be populated by absorption of light according to the Rydberg equation $\nu = R_H[(1/n_2)^2\text{-}(1/n_1)^2]$ with $R_H = 109.677\ cm^{-1}$. R. Mills has hypothesized and experimentally tested that the $n = 1$ state is not the absolute ground state and that lower-energy hydrino states characterized by fractional quantum numbers 1/p, with $2 = p \leq 137$, can exist. The underlying theory has been presented in a series of papers [1–11]. A comprehensive compilation of the theory, known as The Grand Unified Theory of Classical Physics (GUTCP) is available as a 3-vol e-book with regular updates [12]. Ample experimental evidence has been presented by the Mills lab that H(1/p) can be produced from H(n = 1) in a non-radiative process whereby a catalyst reversibly takes up an amount of energy equal to (p-1) × 27.196 eV such that a total amount equal to $(p^2\text{-}1) \times 13.598$ eV is ultimately released as heat, continuum EUV emission, energetic signatures, and hydrino chemical products [13–39], [40–70].

Mills' GUTCP theory has been evaluated – both positively and negatively – by others, however, thus far only on the basis of theoretical arguments [71–84]. Experimental support for the existence of hydrino, as H, H^-, or H_2, has been presented by the Mills lab and other independent laboratories and researchers [13–39], [40–70] using vibrating sample magnetometry, magic angle spinning ^{1}H nuclear magnetic resonance spectroscopy (MAS ^1H NMR), Raman spectroscopy including deuterium substitution, photoluminescence emission spectroscopy, Fourier transform infrared spectroscopy (FTIR), gas chromatography, X-ray photoelectron spectroscopy (XPS), time of flight secondary ion mass spectroscopy (ToF-SIMS), electrospray ionization time of flight mass spectroscopy (ESI-ToFMS), and high performance liquid chromatography (HPLC). The energetics of the hydrino reaction was confirmed by the observation of extraordinarily Doppler and Stark H line broadening, hydrogen plasma afterglow, ultraviolet and visible spectroscopy of population inversion, shockwave formation, 20 MW-level continuum EUV optical power wherein the reaction rate was greatly increased by applying an arc current to recombine ions and electrons formed by the energy transfer to HOH that is consequently ionized, differential scanning calorimetry of hydrino solid-fuel reactant mixtures, electrical energy balance of hydrino reaction electrochemical cells, and water bath calorimetry on so-called SunCells® comprising a molten gallium injector that electrically shorts two plasma electrodes with the molten gallium to maintain an arc current plasma state that boosted output power to 340,000 W in a 0.5 -liter reactor volume. The present study significantly extends this body of research as it is carried out in an independent laboratory with a technique, EPR, not previously applied in hydrino studies.

Experimental

Full experimental details are given in the ESI. These include descriptions of plasma reactor setup, production of reactants, reaction control, and product processing. Analytical methods for product analysis are detailed covering gas chromatography, scanning electron microscopy, energy dispersive X-ray spectroscopy, Rutherford backscattering spectrometry, time-of-flight secondary ion mass spectrometry, transmission electron microscopy, and X-ray diffraction. The EPR spectroscopy is described including all in-house developed software for data analysis.

Results and discussion

Molecular hydrino sample production

A common feature of a hydrino state and an excited H state is that both comprise an electron, a proton, and a photon. In an excited H state, the photon superimposes the proton field to decrease the central field at the electron to + e/n (e is the fundamental charge) and creates a radial dipole instability that results in radiation. Conversely, the photon of a hydrino state increases the central field at the electron to +(1+m)e and creates a radial monopole that is radiatively stable. According to GUTCP, ground-state (n = 1) atomic hydrogen can be converted to atomic hydrino (n = 1/(1+m)) by means of a nonradiative resonant energy transfer to a catalyst with potential energy = m × 27.2 eV (that is 2 m × E_1) according to the reaction

$$m \times 27.2\ eV + H(1) + Cat \rightarrow H^*(1/(1+m)) + Cat^* + m \times 27.2\ eV$$

in which the energy term on the left is energy absorbed by the catalyst (typically by resonant ionization) and the term on the right is the energy released by the increase in the potential energy of the hydrogen atom to form H*(1/(1+m)), an intermediate of the hydrino atom of radius a_H. Subsequently the ionized catalyst, Cat*, regenerates by recombination, with the release of its previously gained ionization energy, and the hydrino intermediate converts to stable H(1/(m+1)) having a radius of $a_H/(1 + m)$ by release of additional energy such that the overall release of energy is $[(m+1)^2\text{–}1] \times 13.6$ eV. By considering the quantum state p = m +1 the reaction may be written

$$H(1) \rightarrow H(1/p) + (p^2\text{-}1) \times 13.6\ eV$$

The hydrino transition reaction requires atomic H and a single catalyst species which is typically formed chemically or by a plasma reaction [13–20]. Further reactivity produces molecular hydrino H_2(1/p) from atomic hydrino H(1/p) when the bond energy is removed by collision with a third body, which can be a reactor-wall constituent [85]. A variety of species can resonantly and nonradiatively accept m × 27.2 eV from atomic hydrogen to serve as catalyst for hydrino formation; in the present case we use the nascent (that is, in situ prepared, not hydrogen-bonded) water molecule with potential energy 3 × 27.2 eV [13,14]. Details of the sample preparation are given in ESI. Briefly, the reactor is a closed vessel in which a low-voltage discharge is created between a liquid gallium electrode and a solid tungsten electrode with water and hydrogen introduced from a supported-Pt H_2/O_2

recombiner supplied with H_2 gas and trace O_2 to form trace nascent, or non-H-bonded water catalyst. Either additional oxygen or water vapor are introduced to produce gallium oxide that is collected. Regular $H_2(1)$ is known to absorb onto Ga_2O_3 [86–88]. It is unknown if molecular hydrino putatively associated with the Ga_2O_3 is sufficiently stable to survive slow transfer to an EPR lab because the Ga_2O_3 collected from the SunCell® reactor is contaminated with metallic gallium along with Ga(O)OH. The presence of gallium metal precludes EPR spectroscopy on the mixture. However, high-purity crystalline Ga(O)OH for EPR analysis is isolated as follows. After dissolution of the mixture of gallium metal, gallium oxide, and Ga(O)OH in 4 M KOH, a unique non-soluble product comprising Ga(O)OH in the form of an aggregate of micro-spheres containing molecular hydrino $H_2(1/4)$ slowly polymerizes as shown by scanning electron microscopy (SEM) and transmission electron microscopy (TEM) in Fig. 1. We denote this stabilized system by $H_2(1/4)$@Ga(O)OH compliant with a common notation for atomic hydrogen occluded in solid hosts [89,90].

Energy dispersive X-ray spectroscopy (EDS) showed an elemental composition of $GaO_{2.1}$ (Fig. S1). Conventional elemental analysis of H relies on combustion to H_2O. However, $H_2(1/4)$ theoretically and experimentally does not undergo combustion with oxygen. The molecular orbital electron energy level is too low to react with oxygen. Therefore, Rutherford backscattering spectrometry (RBS) was performed on the $H_2(1/4)$@Ga(O)OH which identified the composition as $GaO_{1.68}H_{1.32}$ with a density of 8.56×10^{22} atoms/cm^2 corresponding to an excess H content, some of which is hydrino hydrogen, based on the results of gas chromatographic identification and EPR spectroscopy reported below. Time-of-flight secondary ion mass spectrometry (ToF-SIMS), presented in Fig. S2, showed Ga in the positive ion spectrum and O and H as dominant ions in the negative ion spectrum wherein the hydride ion was elevated compared to control Ga(O)OH. No hydrocarbons above adventitious levels were present and no nitrogen was found indicating the unlikeliness for EPR signals to originate from organic radicals. Equally, in the positive spectrum no potentially paramagnetic transition ions were present. Selected area electron diffraction (SAED) with the transmission electron microscope (Fig. S3) revealed the samples to comprise two different morphological and crystalline forms of Ga(O)OH: rods with orthorhombic diffraction pattern matched control Ga(O)OH, which lacks molecular hydrino, in morphology and crystalline structure [91] and were not sensitive to the TEM electron beam; on the other hand, morphologically polymeric crystals comprising hexagonal crystalline structure were very electron-beam sensitive, and were assigned to novel $H_2(1/4)$@Ga(O)OH. X-ray diffraction (XRD) showed a phase shift from the Ga(O)OH control lines with different deviations between NaOH and KOH formed $H_2(1/4)$@Ga(O)OH as illustrated in Fig. S4.

Gas chromatography of molecular hydrino

The $H_2(1/4)$ molecule has a cross section that is circa 1/64 of that of the helium atom. By consequence it is difficult to store molecular hydrino in a container for extended periods of time. Also, the here employed production scheme always results in contamination with regular $H_2(1)$. $H_2(1/4)$ was identified by gas chromatography in two complementary experiments. $H_2(1/4)$ gas was collected from the SunCell® reactor using a valved microchamber connected to the vacuum line and cooled to 15 K by a cryopump system. The liquefied gas was warmed to room temperature to achieve 10 Torr chamber pressure and was injected into a gas chromatograph. $H_2(1/4)$ was observed as an early peak at 8.31 min and hydrogen that co-condensed with H_2 gas was observed at 12.87 min (Fig. 2a).

The peak at 18.24 min is oxygen that was condensed before the SunCell® run to serve as a solvent for $H_2(1/4)$. The collected gas contained no helium by mass spectroscopy. The early peak was negative with a helium carrier gas indicating that the early peak had a higher thermal conductivity, and the migration rate was faster than that of helium with an argon carrier gas. No known gas has a faster migration rate and higher thermal conductivity than H_2 or He, which is characteristic of and identifies hydrino since it has a much greater mean free path due to exemplary $H_2(1/4)$ having 64 times smaller volume and 16 times smaller ballistic cross section. Hydrogen condensed under pressure and temperature conditions that violate the Clausius Clapeyron equation due to the

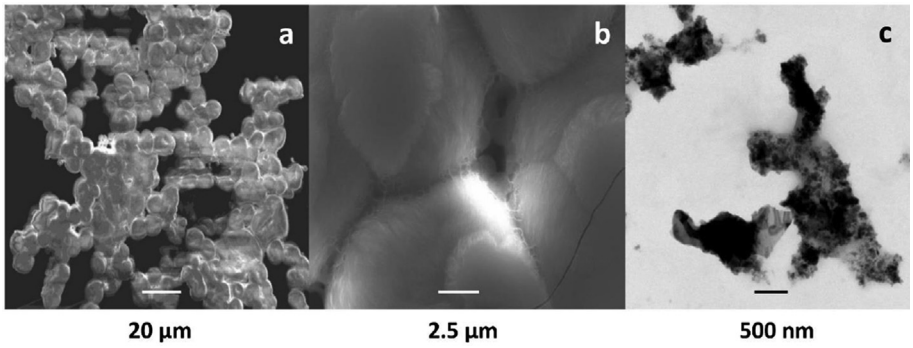

Fig. 1 – Scanning electron microscopy and transmission electron microscopy of $H_2(1/4)$@Ga(O)OH. Trace a: SEM at 800 × magnification showing chains of microspherical particles; trace b: SEM showing 5 μm width of the particles, each comprising very fine fibers; trace c: TEM imaging of morphologically polymeric crystals of hexagonal structure (Fig. S3), which were very sensitive to the TEM electron beam. Observed spherical particles have approximately 100 nm average diameter.

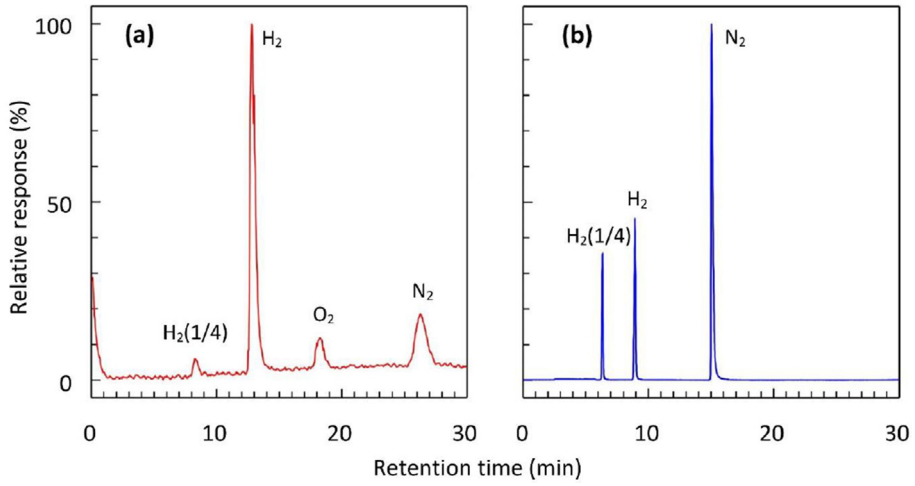

Fig. 2 – Gas chromatographic identification of molecular hydrino $H_2(1/4)$. Trace a: GC of gas collected from the SunCell® reactor with a cryopump showing $H_2(1/4)$ at 8.31 min. Trace b: the GC of hydrino gas evolved by heating the KOH-treated Ga_2O_3/Ga(O)OH material collected from the SunCell® to 800 °C. The known hydrogen and nitrogen peaks were observed at ca 8 and 15 min and a novel peak at ca 6 min was assigned to $H_2(1/4)$.

raising of the H_2 liquefaction temperature by co-condensation with $H_2(1/4)$.

In a different experiment gas chromatography was performed on the gases released by thermal desorption of gas bound to the KOH-treated Ga_2O_3/Ga(O)OH sample originally collected from a SunCell® plasma run. Known gases such as hydrogen were also run to identify their migration times to compare to the results of the SunCell®-derived sample. The gas chromatograph of hydrino gas evolved by heating the Ga(O)OH material to 800 °C is shown in Fig. 2b. Note that the amplitudes of the peaks assigned to molecular hydrino in the experiments of Fig. 2 are not quantifiable: since $H_2(1/4)$ is not obtained in pure form, its effect on the thermal conductor sensor cannot be quantified.

Paramagnetism of molecular hydrino

Alternative to the probabilistic matter waves of quantum mechanics, the electron in a hydrogen atom is modelled in GUTCP as a two-dimensional spherical membrane of infinitesimal thickness in which current flows along two infinite, nested rotation sets of great circle filaments. This current pattern naturally gives rise to both orbital and spin angular momentum wherein the latter defines a free-electron factor $g_e = 2.0023193$ [3,4,7–9,12,13]. In the hydrogen molecule the spherical current pattern becomes a prolate spheroid in which the pairing of two electrons leads to a diamagnetic ground state. Atomic hydrino differs from H(n > 1) states in that rather than the absorption of a photon to form an excited state, H(n = 1/p) is formed by a non-radiative energy transfer to a resonant energy acceptor followed by continuum extreme ultraviolet radiation to the final stable hydrino atomic state. Two hydrino atoms react to form molecular hydrino having two photons that are phase-locked to the electron current and circulate in opposite directions. Consequently, the molecule has a diamagnetic and a paramagnetic electron, the latter with $g \neq g_e$ equal to $2 + 2 \times 0.0023193 = 2.0046386$ [92]. This fundamental prediction from first principles provides a unique, simple, and accurate testing criterion for the existence of molecular hydrino. Moreover, the theory predicts a specific and detailed splitting, or fine structure, of the g = 2.00464 resonance into a multi-line pattern due to internal magnetic and spin-orbit couplings affording a distinguishing EPR signature of molecular hydrino $H_2(1/4)$.

EPR spectroscopy of molecular hydrino

A wide magnetic field scan EPR spectrum of the Ga(O)OH solid powder taken at ambient temperature, exhibits a single derivative feature only against an essentially flat background, and with g value close to the free-electron value (Fig. 3a).

Zooming-in on this feature (Fig. 3b) shows it to consist of two separate lines plus multiple weak signals in the low- and high-field wings. The center of the two main lines corresponds to an apparent g value of 2.0045(6) which is close to the value of 2.00464 predicted for the $H_2(1/4)$ S = 1/2 spin-only doublet system. The two lines are separated by circa 4 gauss and are of equal intensity. Microwave power saturation plots (Fig. S5) are very similar for the two peaks and are consistent with inhomogeneous broadening [93] (see below).

Concentrating on resolving fine structure in the main peaks we reduce the magnetic-field modulation amplitude to 25 mG (that is, below the bandwidth of the 100 kHz modulation frequency). The spectral amplitude in a single scan drops to below a signal-to-noise ratio of unity and extensive averaging over 6 h and filtering is required to afford the high-resolution pattern in Fig. 3c. Each line has resolved in an isotropic equidistant beat pattern with sub-line separation of circa 0.32 gauss.

For individual sub-lines we observe an apparent peak-to-peak width of circa 170 mG which is highly unusual for solid-state samples. Such narrow lines have only been found for (i) organic radicals in organic solvents at ambient temperature [94]; (ii) small paramagnetic molecules in matrices of

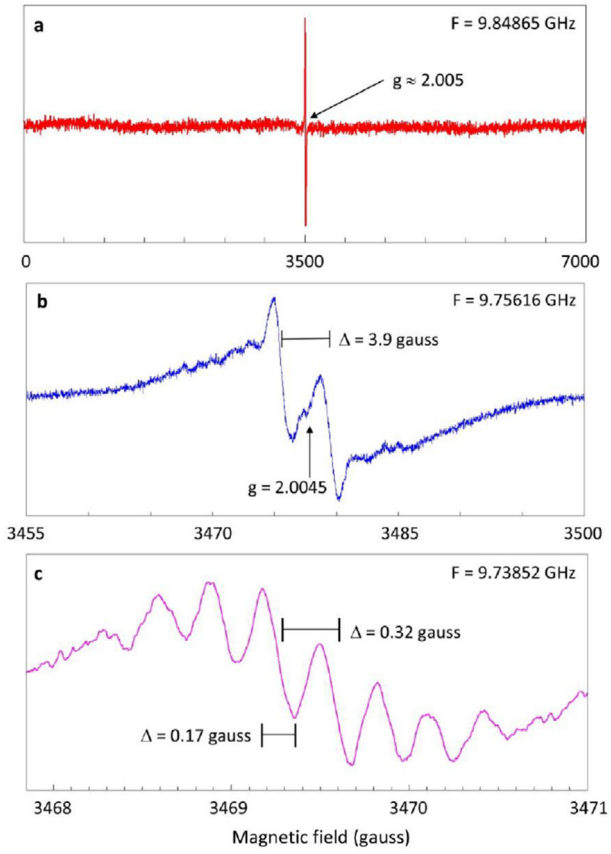

Fig. 3 – EPR of postulated molecular hydrino $H_2(1/4)$ caged in solid Ga(O)OH polymer. Trace a: wide-scan overview spectrum showing a single feature only close to the free electron g value. Trace b: zoom-in of the single feature in trace a shows two main lines of equal intensity, separated by circa 4 gauss, and whose center is distinctly shifted from the free electron value to g = 2.0045. Trace c: further zoom-in on one of the lines now recorded with a very small modulation amplitude reveals a fine structure of multiple lines with apparent peak-to-peak derivative line width of 0.17 gauss and separated by circa 0.32 gauss. Data collection times for traces a-c were 10, 16, and 375 min, respectively. Modulation amplitudes were 1, 1, and 0.25 gauss, respectively. All spectra were taken at ambient temperature. Other experimental conditions are given in ESI.

noble gasses solidified at cryogenic temperatures [95]; (iii) single hydrogen atoms encapsulated in molecular cages [96]; and (iv) paramagnetic molecules in the gas phase at low pressure [97]. Excluding the first two options on obvious grounds (no organic solvents and no cryogenic temperatures) and the third one on spectroscopic grounds (atomic hydrogen EPR is a single line at the free electron g_e value split by over 500 gauss through proton hyperfine interaction), the narrow line width that we observe would only be consistent with the detection of a low-pressure paramagnetic gas occluded in a solid.

We recorded the spectrum in Fig. 4a under optimized conditions for the detection and resolution of satellite lines whose existence was indicated by the small periodic peaks in the wings of the spectrum in Fig. 3b. Thus, the fine structure of the two central lines was slightly deformed by over-modulation, and the data collection was extended to 40 h with constant frequency monitoring for subsequent correction of individual 4-min traces for minor frequency drift. The spectrum has been reproduced completely in duplicate on two different spectrometers in a lab of the spectrometer's manufacturer (Bruker, Billerica, MA, USA) [13]. The spectrum of Fig. 4a is stable for at least two years; it is reproducible over 11 samples produced in 11 reactor runs (Fig. S6), and the spectrum of an empty tube is a straight baseline (Fig. S6).

In spin quantification (ESI) we find that a complete spectrum of high resolution, such as in Fig. 4a, represents an S = 1/2 concentration of circa 2.6 μM if the paramagnet would be homogeneously distributed over the sample volume. Transmission electron microscopy (Fig. 1) and XRD show the Ga(O)OH polymer to comprise micro-spherical particles of the order of 100 nm diameter with an estimated spatial occupancy of roughly 10%. This would make the actual concentration of the $H_2(1/4)$ gas in occlusion very approximately 26 μM, which is equivalent to a partial pressure of circa 6×10^{-4} bar, qualitatively consistent with the observed narrow EPR line width [94,98]. Even if regular H_2 would co-occlude at, say, atmospheric pressure the small cross section for collision of molecular hydrino $H_2(1/4)$ would ensure a low collision frequency in agreement with the observed line width.

Simulation of the fine structure in spectrum Fig. 3c indicated the line shape to be Gaussian within the limitation set by the overlap of individual lines. The sets of satellite lines are better separated, and analysis of the first down-field triplet

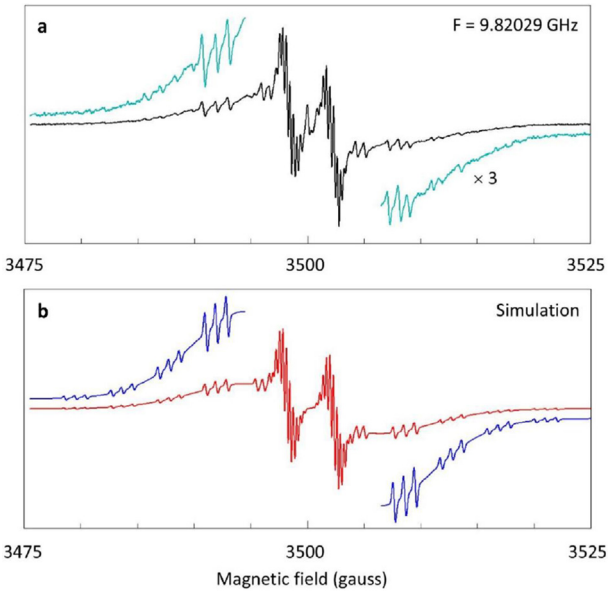

Fig. 4 – Full EPR spectrum at high resolution of molecular hydrino $H_2(1/4)$. Trace a: extensively averaged spectrum (2400 min) taken under conditions optimized for maximal signal-to-noise ratio at the expense of minor over-modulation (0.2 gauss), exhibits a complex pattern of triplet satellite lines. Trace b is a simulation using field positions predicted by hydrino theory.

clearly shows the line shape to be essentially Gaussian (Fig S7). This implies inhomogeneous broadening, consistent with the power-saturation analysis (Fig. S5), and could be caused by interaction of hydrino molecules with the inner 'wall' of the inorganic polymer cage. In turn, this would imply the real lifetime line width from gas collision to be significantly less than the observed 170 mG inhomogeneous line width.

Interpretation of molecular hydrino EPR

Molecular hydrino comprises two protons at the foci of a two-electron prolate spheroid molecular orbital membrane, and an absorbed photon. The latter splits into two photons that are phase locked with the oppositely directed current patterns of the two electrons each consisting of an angularly distributed infinite ensemble of closed grand ellipse filaments of moving charge of an equipotential, minimum energy membrane surface [92]. Under this model exact solutions of a fine structure in the EPR ensues with parameters whose predicted magnitudes can be tested against experimental values.

The unique electronic structure results in one paramagnetic and one diamagnetic electron. The former induces a current in the latter by means of spin-orbit coupling resulting in a split of the original resonance into two lines separated by a frequency-independent interaction, which is for $H_2(1/4)$ predicted to be of magnitude 3.9943 gauss with the field center of the two lines corresponding to the original g value of 2.00464 [92]. Experimentally we observe two lines of equal intensity separated by 3.9 gauss whose center is found at $g = 2.0045(6)$.

Linkage of magnetic flux by the electron is quantized in units of the magnetic flux quantum $\varphi_0 = h/2e$, which results in a sub-line pattern of each of the two main lines with a predicted separation of 0.311 gauss [92]. The observed separation is 0.32 gauss.

Similar to the case of excited-states of the regular H_2 molecule, the two electrons in $H_2(1/4)$ may rotate relative to each other along the semimajor axis during a spin transition. The relative rotation is quantized in terms of m integer units of $\hbar$ in opposite directions with the spin-orbit splitting in frequency-independent field units equal to $\pm$ m times twice the splitting between the two main lines, that is $\pm m \times 7.9885$ gauss. Additionally, the unpaired electron must link the magnetic flux component corresponding to spin-orbit coupling. This flux contribution increases the magnetic energy and the energy of the combined spin flip and spin-orbit coupling transition energy for a given spin-orbital quantum number m. Thus the downfield spin-orbital splitting peaks are shifted further downfield by the corresponding magnetic energies, whereas the upfield spin-orbital splitting peaks are not shifted since they correspond to emission of the spin-orbital coupling transition energies alone.

Furthermore, each of these satellite lines is split through the linkage of magnetic flux during a spin transition, and the exact solution of the splitting is circa 0.62 gauss for $|m| = 1$ and circa 0.93 for $|m| > 1$ where the latter lines follow an intensity pattern $I_{m+1}/I_m = m/(m+2)$. The predicted details [92] of this complex pattern of split satellite lines asymmetrically grouped around a g value of 2.00464 make up a stick spectrum that, when convoluted with a Gaussian derivative, forms a semi-quantitative reproduction of the experimental spectroscopy (Fig. 4b and Table I).

Checks on consistency of EPR interpretation

Unequivocal interpretation of complex EPR spectra typically requires analysis of data taken at more than one microwave frequency. The magnetic model of molecular hydrino $H_2(1/4)$, providing a basis for interpretation of the EPR, predicts a number of features to be either dependent or independent of microwave frequency. These predictions can be checked in separate experiments as consistency tests. The g value of 2.00464 in between the two main lines is a real g value and thus its field position should be linear in the microwave frequency. Contrarily, all fine structure splittings are predicted to be constant in field units and thus independent of the frequency.

As a check we have taken data in Q-band at circa 35 GHz. Here, practical complications arise resulting in reduced signal-to-noise ratios. For $S = 1/2$ systems, any spectrometer operating in a frequency band different from X-band is generally found to exhibit a significantly lower concentration sensitivity. Furthermore, the maximal applicable intensity of the microwave is found to be limited (that is, the spectrometer is not tunable at higher microwave powers) apparently due to a relatively high dielectric permittivity of the Ga(O)OH samples.

Fig. 5 shows two traces resulting from extensive averaging, one taken under over-modulating conditions to emphasize the main two-line pattern, and one taken at lower modulation amplitude in an attempt to resolve fine structure. Consistent with the interpretation of the X-band spectrum we find a doublet of lines whose spectral center has a real g value of 2.0046 and with a frequency-independent splitting of circa 4 gauss. Under the employed conditions, the underlying broad signal has turned dispersive and thus shows up as an absorption-shape feature. A lower modulation amplitude

Table I – Comparison of experimental and theoretical EPR peak positions of molecular hydrino. The experimental magnetic-field values are taken from the spectrum at 9.82029 GHz (Fig. 4a) as peak positions of the center line of 11 multiplets. The theoretical values [92] are due to the electron spin-orbit coupling splitting energies for downfield and upfield spin-orbit coupling quantum numbers m = 0, 0.5, 1, 2, 3, 4. All values are in gauss.

m	experimental	theoretical	difference
4	3480.5	3481.24	−0.74
3	3486.8	3486.50	0.30
2	3491.7	3491.39	0.31
1	3495.7	3495.93	−0.23
0.5	3498.5	3498.06	−0.44
0	3500.4	3500.10	0.30
0.5	3502.3	3502.10	0.20
1	3504.0	3504.09	−0.09
2	3507.8	3508.09	−0.29
3	3511.5	3512.08	−0.58
4	3517.3	3516.08	1.22
Average (st. dev.):	−0.004 ± 0.550		

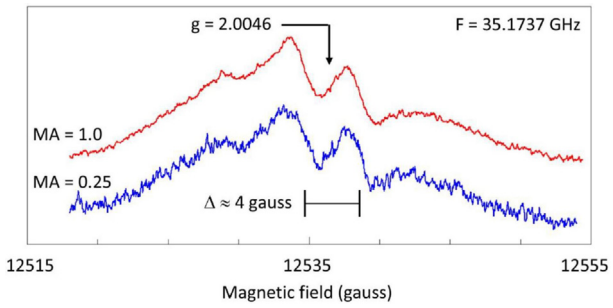

Fig. 5 – A 35 GHz frequency experiment as check on consistency of the EPR interpretation: extensively averaged Q-band spectra taken at two different modulation amplitudes (MA) of 1 gauss (red) or 250 mG (blue). No fine structure is resolved in addition to the two main lines consistent with an inhomogeneous line width linear in the microwave frequency. The central g value and the splitting between the two lines in field units are identical to those observed in X-band. See ESI for other experimental conditions.

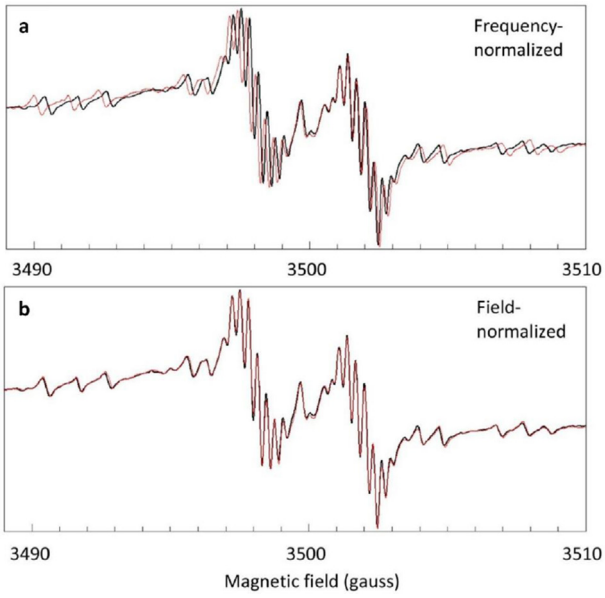

Fig. 6 – In-band dual frequency experiment as check on consistency of the EPR interpretation. Trace a: extensively averaged intra X-band experiment at two frequencies, 9.4629 GHz (red) and 9.8209 GHz (black). Each field point of the red spectrum is frequency transformed to that of the black spectrum where the overlay shows that only the center of the two main lines is a real g value. In trace b the red spectrum is shifted in its entirety to a higher field for maximal overlap with the black spectrum. Here the overlay proves that there is only a single real g value and that all other features are constant in the field.

does not afford resolution of the two-lines' fluxonal fine structure, which indicates that the spectral line width has increased with frequency. This is in fact consistent with our previous conclusion (cf. Fig 2c and Fig. S7) that the line shape is Gaussian due to inhomogeneous broadening, which implies a line width in field units linear in frequency [99].

Since the signal-to-noise ratio in Q-band was insufficient to detect the satellite lines, and since attempts to measure the samples in other frequency bands were hitherto unsuccessful (not shown), we took data at two, well-separated frequencies within the X-band thus allowing for comparison of high-resolution spectra with the trade-off of reduced frequency resolution (Fig. 6ab). Data taken at 9.46 GHz were transformed for comparison with data taken at 9.85 GHz in two ways: (1) frequency-ratio conversion of every digital point of the field axis, and (2) single-valued overall field shift to create maximal overlap of the two spectra. In the first method all real g values will overlay while features constant in the field will mismatch. In the second method all features of a fine-structure pattern constant in the field will overlay when the selected field point of conversion corresponds to the g value of that pattern. Fig. 6a gives the result of the first method: all features mismatch except for the spectral center at g = 2.0046, therefore the latter is the only real g value and all other features are from frequency-independent hyperfine interactions. Fig. 6b gives the result of the second method: all lines match, including all satellite lines and all fluxon sub-lines of the two main lines, therefore all features are from frequency-independent hyperfine interactions and they all share a single, common g value.

Search for alternative interpretation of the EPR

Alternative to the hydrino analysis in Fig. 4b the spectrum in Fig. 4a can also be approximately reproduced under a conventional phenomenological spin Hamiltonian assuming an unusual combination of two isotropic radicals of unequal intensity each with a g value of 2.0046. This model would require the two main lines to be due to an isotropic S = 1/2 system split by an I = 1/2 nucleus with $A_{iso} \approx 3.9$ gauss with additional hyperfine structure form a combination of some five nuclei the majority of which has also I = 1/2. A second S = 1/2 system should give rise to the satellite lines due to a different combination of five nuclei, one of which should have I = 1 (e.g. ^{14}N) to account for the repeating triplet pattern (see Fig. S8 for a detailed analysis).

In addition to the improbability of the above combination of spin Hamiltonian parameters we consider this alternative explanation of the EPR highly unlikely on the following grounds. The reaction mixture only contains H_2, O_2, H_2O, and Ga. Even in the presence of trace contaminants we cannot envision how the high-temperature plasma reaction conditions and sample formation in strong aqueous base could lead to the formation of stable radical structures of considerable complexity. The ToF-SIMs, EDS, and XRD analyses also eliminate alternatives. Furthermore, since the sample is a solid, for complex radicals one would expect to see anisotropy in the spectra. In particular absorption-shaped peaks that come with axial or rhombic symmetry of the spin Hamiltonian are not observed. Finally, when the sample temperature is lowered below ambient, relaxation of the two main peaks becomes distinct (Fig. S9), which would be hard to reconcile with a nuclear hyperfine doublet assignment.

Remaining questions

The GUTCP fit to the X-band spectrum of $H_2(1/4)$ is semi-quantitative with an average error of 0.004 ± 0.550 gauss over the 11 lines assigned to spin-orbital coupling splitting. The actual positions of the satellite lines slightly deviate from their predicted values (Fig. 4a, b and Table I). Also, the fluxon separation for any given position does not quantitatively fit the predicted value; in particular the separation is not a constant. Also, the number and relative intensities of fluxon lines for a given satellite line are presently not understood. Possibly these small irregularities are caused by interactions of the gaseous $H_2(1/4)$ with the wall of the polymeric Ga(O)OH microspheres.

A broad signal underlies the molecular-hydrino assigned spectrum. Its spectral center corresponds to the g value of 2.0046 within experimental error. Its temperature behavior is very different from that of the hydrino-assigned spectrum (Fig. S10). The origin and nature of the broad signal are presently unknown, however, a reasonable hypothesis would be to assume that there are two phases of Ga(O)OH that encapsulate $H_2(1/4)$ wherein $H_2(1/4)$ is a near free gas in only one phase. A scanning/transmission electron microscope (SEM/TEM) used for imaging and selected area electron diffraction (SAED) (Fig. S3) showed that the $H_2(1/4)$@Ga(O)OH sample comprised two different morphologically polymeric crystals of Ga(O)OH, a hexagonal crystalline structure that was very sensitive to the TEM electron beam, and rods having orthorhombic crystalline structure that were not electron beam sensitive. The rod crystal morphology and crystalline structure match those of the literature for control Ga(O)OH that lacks gaseous molecular hydrino inclusion [91]. The XRD crystal system for tsumgallite (control Ga(O)OH) is orthorhombic. The hexagonal phase is likely the source of the fine structure EPR spectrum, and the orthorhombic phase is likely the source of the broad background EPR feature. Cooling selectively eliminates, by microwave power saturation, the observed near free-gas-like EPR spectral behavior of $H_2(1/4)$ trapped in the hexagonal crystalline matrix. In addition to wall interactions, deviations from theory could be due to the influence of the proton of Ga(O)OH and those of absorbed water. Also, matrix orientation in the magnetic field, matrix interactions, and interactions between one or more $H_2(1/4)$ could cause some shifts.

Deuterium substitution was performed to eliminate an alternative assignment of any EPR spectral lines as being nuclear split lines. Rotational-nuclear interaction was predicted to be absent since the experimentally confirmed theoretical rotation energy of $H_2(1/4)$ is 16 times that of H_2, too high to be excited at ambient temperatures [12,13]. The EPR spectrum of the deuterated analog HD(1/4)@Ga(O)OH showed a singlet with no fine structure (Fig S11); thus, eliminating any possible nuclear splitting assignment. The g factor and profile matched that of the singlet of $H_2(1/4)$ @Ga(O)OH wherein the singlet in both cases was assigned to the orthorhombic phase. The XRD of the deuterated analog matched that of the hydrogen analog, both comprising gallium oxyhydroxide. TEM confirmed that the deuterated analog comprised 100% orthorhombic phase [91]. The phase preference of the deuterated analog may be due to a different hydrino concentration and kinetic isotope effect which could have also reduced the concentration.

Conclusions

A plasma reaction has been carried out intended to produce molecular hydrino using non hydrogen bonded water as the catalyst and with liquid gallium as one of the electrodes. Polymeric Ga(O)OH with a spherical particle structure, presumably containing $H_2(1/4)$, was purified from the reaction mixture. $H_2(1/4)$ is proposed to be an $S = 1/2$ paramagnet with complex fluxonal and spin-orbital coupling sub-level structure. The solid Ga(O)OH compound exhibits a complex gas-phase X-band EPR spectrum at ambient temperature whose fine structure semi-quantitatively agrees with hydrino-theory predictions. This analysis is consistent with frequency-dependent studies, while alternative, conventional interpretations are judged to be extremely unlikely. In summary, the present study provides compelling EPR spectroscopic and gas chromatographic evidence for the existence of molecular hydrino, and, by inference, for the reality of atomic hydrino, and it provides plausibility of the electron model in GUTCP. In more general terms our results are a significant test against falsification of GUTCP. In view of the possible far-reaching implications of this conclusion for the theory of quantum mechanics, for hydrogen-related chemistry, for astrophysics of dark matter, and for energy transduction and production technology, it is also offered as an urgent invitation to academia at large to repeat and extend the described experiments in lieu of refutation on quantum mechanical theoretical grounds. An early version of the present paper has been posted on a preprint server [100].

Author contributions

RLM developed the theory and was responsible for the production and analysis of the samples; WRH did the EPR experiments and analyses and wrote the dedicated software; WRH and RLM wrote the manuscript.

Declaration of competing interest

The authors declare the following financial interests/personal relationships which may be considered as potential competing interests:

Dr. Mills is the founder, CEO, and President of Brilliant Light Power which provided the samples for independent analyses except for the gas chromatography which was performed in house. Dr. Hagen has no financial or personal relationships and did not receive and financial support from Brilliant Light Power.

Acknowledgement

We are grateful to Dr Peter van Noorden for creating the liaison between the authors.

Appendix A. Supplementary data

Supplementary data to this article can be found online at https://doi.org/10.1016/j.ijhydene.2022.05.156.

REFERENCES

[1] Mills RL. The hydrogen atom revisited. Int J Hydrogen Energy 2000;25:1171–83.
[2] Mills RL. The nature of free electrons in superfluid helium – a test of quantum mechanics and a basis to review its foundations and make a comparison to classical theory. Int J Hydrogen Energy 2001;26:1059–96.
[3] Mills RL. The grand unified theory of classical quantum mechanics. Int J Hydrogen Energy 2002;27:565–90.
[4] Mills RL. Classical quantum mechanics. Phys Essays 2003;16:433–98.
[5] Mills RL. The nature of the chemical bond revisited and an alternative Maxwellian approach. Phys Essays 2004;17:342–89.
[6] Mills RL. The fallacy of Feynman's and related arguments on the stability of the hydrogen atom according to quantum mechanics. Ann Fond Louis Broglie 2005;30:129–50.
[7] Mills RL. Exact classical quantum-mechanical solutions for one- through twenty-electron atoms. Phys Essays 2005;18:321–61.
[8] Mills RL. Maxwell's equations and QED: which is fact and which is fiction? Phys Essays 2006;19:225–62.
[9] Mills RL. Physical solutions of the nature of the atom, photon, and their interactions to form excited and predicted hydrino states. Phys Essays 2007;20:403–60.
[10] Mills RL. Exact classical quantum mechanical solution for atomic helium which predicts conjugate parameters from a unique solution for the first time. Phys Essays 2008;21:103–41.
[11] Mills RL, Holverstott B, Good B, Hogle N, Makwana A. Total bond energies of exact classical solutions of molecules generated by MILLSIAN 1.0 compared to those computed using modern 3-21 G and 6-31 G* basis sets. Phys Essays 2010;23:153–99.
[12] Mills RL. The grand unified theory of classical Physics. 2020. three vol. s, www.brilliantlightpower.com/book-download-and-streaming/.
[13] R. Mills, Hydrino states of hydrogen, submitted; https://brilliantlightpower.com/pdf/Hydrino_States_of_Hydrogen.pdf.
[14] Mills R, Lu Y, Frazer R. Power determination and hydrino product characterization of ultra-low field ignition of hydrated silver shots. Chin J Phys 2018;56:1667–717.
[15] Mills RL, Lu Y. Hydrino continuum transitions with cutoffs at 22.8 nm and 10.1 nm. Int J Hydrogen Energy 2010;35:8446–56. https://doi.org/10.1016/j.ijhydene.2010.05.098.
[16] Mills RL, Lu Y, Akhtar K. Spectroscopic observation of helium-ion- and hydrogen-catalyzed hydrino transitions. Cent Eur J Phys 2010;8:318–39. https://doi.org/10.2478/s11534-009-0106-9.
[17] Mills RL, Lu Y. Time-resolved hydrino continuum transitions with cutoffs at 22.8 nm and 10.1 nm. Eur. Phys. J. D 2011;64:65. https://doi.org/10.1140/epjd/e2011-20246-5.
[18] Mills RL, Booker R, Lu Y. Soft X-ray continuum radiation from low-energy pinch discharges of hydrogen. J Plasma Phys 2013;79:489–507. https://doi.org/10.1017/S0022377812001109.
[19] A. Bykanov, "Validation of the observation of soft X-ray continuum radiation from low energy pinch discharges in the presence of molecular hydrogen," http://www.blacklightpower.com/wp-content/uploads/pdf/GEN3_Harvard.pdf.
[20] Mills R, Lotoski J, Lu Y. Mechanism of soft X-ray continuum radiation from low-energy pinch discharges of hydrogen and ultra-low field ignition of solid fuels. Plasma Sci Technol 2017;19:1–28.
[21] van Gessel AFH, Thesis Masters. EUV spectroscopy of hydrogen plasmas. April. EPG 09-02. Eindhoven University of Technology, Department of Applied Physics, Group of Elementary Processes in Gas Discharges; 2009. p. 61–70.
[22] Lotoski R Mills J. H_2O-based solid fuel power source based on the catalysis of H by HOH catalyst. Int'l J. Hydrogen Energy 2015;40:25–37.
[23] Mills RL, Lotoski J, Zhao G, Akhtar K, Chang Z, He J, Hu X, Wu G, Chu G, Lu Y. Identification of new hydrogen states. Phys Essays 2011;24:95–117. https://doi.org/10.4006/1.3544207.
[24] Kuraica M, Konjevic N. Line shapes of atomic hydrogen in a plane-cathode abnormal glow discharge. Phys Rev 1992;46(7):4429–32. October.
[25] Kuraica M, Konjevic N, Platisa M, Pantelic D. Plasma diagnostics of the Grimm-type glow discharge. Spectrochim Acta 1992;47:1173–86.
[26] Videnovic IR, Konjevic N, Kuraica MM. Spectroscopic investigations of a cathode fall region of the Grimm-type glow discharge. Spectrochim Acta, Part B 1996;51:1707–31.
[27] Alexiou S, Leboucher-Dalimier E. Hydrogen Balmer-α broadening in dense plasmas. Phys, Rev. E 1999;60(3):3436–8.
[28] Djurovic S, Roberts JR. Hydrogen Balmer alpha line shapes for hydrogen-argon mixtures in a low-pressure rf discharge. J Appl Phys 1993;74(No. 11):6558–65.
[29] Radovanov SB, Dzierzega K, Roberts JR, Olthoff JK. Time-resolved Balmer-alpha emission from fast hydrogen atoms in low pressure, radio-frequency discharges in hydrogen. Appl Phys Lett 1995;66(No. 20):2637–9.
[30] Radovanov SB, Olthoff JK, Van Brunt RJ, Djurovic S. Ion kinetic-energy distributions and Balmer-alpha (H_α) excitation in $Ar - H_2$ radio-frequency discharges. J Appl Phys 1995;78(2):746–57.
[31] Baravian G, Chouan Y, Ricard A, Sultan G. Doppler-broadened H_α lineshapes in a rf low-pressure H_2 discharge. J Appl Phys 1987;61:5249–53.
[32] Ayers EL, Benesch W. Shapes of atomic hydrogen lines produced at a cathode surface. Phys. Rev. 1988;A37:194–9.
[33] Phelps AV. Collisions of H^+, H_2^+, H_3^+, ArH^+,H^-, H, and H_2 with Ar and Ar^+ of ArH^+ and H_2 with for energies from 0.1 eV to 10 keV. J Phys Chem Ref Data 1992;21:883–97.
[34] Barton D, Bradley JW, Steele DA, Short RD. Investigating radio frequency plasmas used for the modification of polymer surfaces. J Phys Chem B 1999;103:4423–30.
[35] Cvetanovic N, Kuraica MM, Konjevic N. Excessive Balmer line broadening in a plane cathode abnormal glow discharge in hydrogen" Journal of Applied Physics, vol. 97; 2005. 33302-1 to 33302-8.

[36] Barbeau C, Jolly J. Spectroscopic investigation of energetic atoms in a DC hydrogen glow discharge. Journal of Physics, D, Applied Physics 1990;23:1168–74.

[37] Bzenic SA, Radovanov SB, Vrhovac SB, Velikic ZB, Jelenkovic BM. On the mechanism of Doppler broadening of H_β after dissociative excitation in hydrogen glow discharges. Chem Phys Lett 1991;184:108–12.

[38] Ayers EL, Benesch W. Shapes of atomic-hydrogen lines produced at a cathode surface. Phys Rev 1988;37(No. 1):194–9.

[39] Benesch W, Li E. Line shapes of atomic hydrogen in hollow-cathode discharges. Opt Lett 1984;9(No. 8):338–40.

[40] Bogaerts A, Gijbels R. Effects of adding hydrogen to an argon glow discharge: overview of some relevant processes and some quantitative explanations. Journal of Analytical Atomic Spectroscopy 2000;15:441–9.

[41] Kurunczi P, Shah H, Becker K. Hydrogen Lyman-α and Lyman-β emissions from high-pressure microhollow cathode discharges in Ne-H_2 mixtures. Journal of Physics B: Atomic, Molecular and Optical Physics 1999;32(22):L651–8.

[42] Akhtar K, Scharer J, Mills RL. Substantial Doppler broadening of atomic hydrogen lines in DC and capacitively coupled RF plasmas. J Phys D Appl Phys 2009;42(13):135207. 12pp.

[43] Mills RL, Akhtar K. Tests of features of field-acceleration models for the extraordinary selective H balmer α broadening in certain hydrogen mixed plasmas. Int J Hydrogen Energy 2009;34:6465–77.

[44] Mills RL, Dhandapani B, Akhtar K. Excessive balmer α line broadening of water-vapor capacitively-coupled RF discharge plasmas. Int J Hydrogen Energy 2008;33:802–15.

[45] Phillips J, Chen CK, Mills R. Evidence of energetic reactions between hydrogen and oxygen species in RF generated H_2O plasmas. Int J Hydrogen Energy 2008;33:2419–32.

[46] Phillips J, Chen C-K, Akhtar K, Dhandapani B, Mills R. Evidence of catalytic production of hot hydrogen in RF generated hydrogen/argon plasmas. Int J Hydrogen Energy 2007;32(14):3010–25.

[47] Mills R, Ray P, Dhandapani B. Evidence of an energy transfer reaction between atomic hydrogen and argon II or helium II as the source of excessively hot H atoms in RF plasmas. J Plasma Phys 2006;72(4):469–84. 24.

[48] Mills RL, Ray PC, Mayo RM, Nansteel M, Dhandapani B, Phillips J. Spectroscopic study of unique line broadening and inversion in low pressure microwave generated water plasmas. J Plasma Phys 2005;71:877–88. Part 6.

[49] Mills RL, Akhtar K. Fast H in hydrogen mixed gas microwave plasmas when an atomic hydrogen supporting surface was present. Int J Hydrogen Energy 2010;35:2546–55. https://doi.org/10.1016/j.ijhydene.2009.12.148.

[50] Chen C, Wei T, Collins LR, Phillips J. Modeling the discharge region of a microwave generated hydrogen plasma. J Phys D Appl Phys 1999;32:688–98.

[51] Mills R, Ray P, Mayo RM. CW HI laser based on a stationary inverted lyman population formed from incandescently heated hydrogen gas with certain group I catalysts. IEEE Trans Plasma Sci 2003;31(2):236–47.

[52] Mills RL, Ray P. Stationary inverted lyman population formed from incandescently heated hydrogen gas with certain catalysts. J Phys D Appl Phys 2003;36:1504–9.

[53] Mills R, Ray P, Mayo RM. The potential for a hydrogen water-plasma laser. Appl Phys Lett 2003;82(11):1679–81.

[54] Ulrich A, Wieser J, Murnick DE. Excimer formation using low energy electron beam excitation", second international conference on atomic molecular pulsed lasers, vol. 3403. Proc SPIE; 1998. p. 300–7.

[55] Mills RL, Akhtar K, Zhao G, Chang Z, He J, Hu X, Chu G. Commercializable power source using heterogeneous hydrino catalysts. Int J Hydrogen Energy 2010;35:395–419. https://doi.org/10.1016/j.ijhydene.2009.10.038.

[56] Mills RL, Ray P. A comprehensive study of spectra of the bound-free hyperfine levels of novel hydride ion H^-(1/2), hydrogen, nitrogen, and air. Int J Hydrogen Energy 2003;28(No. 8):825–71.

[57] Mills R, Good W, Jansson P, He J. Stationary inverted lyman populations and free-free and bound-free emission of lower-energy state hydride ion formed by and exothermic catalytic reaction of atomic hydrogen and certain group I catalysts. Cent Eur J Phys 2010;8:7–16. https://doi.org/10.2478/s11534-009-0052-6.

[58] Mills RL, Ray P. Stationary inverted lyman population and a very stable novel hydride formed by a catalytic reaction of atomic hydrogen and certain catalysts. J. Opt. Mat. 2004;27:181–6.

[59] Mills RL, Ray PC, Mayo RM, Nansteel M, Good W, Jansson P, Dhandapani B, He J. Hydrogen plasmas generated using certain group I catalysts show stationary inverted lyman populations and free-free and bound-free emission of lower-energy state hydride. Res. J. Chem Env. 2008;12(2):42–72.

[60] Mills R, Lotoski J, Good W, He J. Solid fuels that form HOH catalyst. Int J Hydrogen Energy 2014;39:11930–44. https://doi.org/10.1016/j.ijhydene.2014.05.170.

[61] Mills R, Yu X, Lu Y, Chu G, He J, Lotoski J. Catalyst induced hydrino transition (CIHT) electrochemical cell. Int J Energy Res 2012. https://doi.org/10.1002/er.3142 (2013).

[62] Mills RL, He J, Chang Z, Good W, Lu Y, Dhandapani B. Catalysis of atomic hydrogen to novel hydrogen species H^-(1/4) and H_2(1/4) as a new power source. Int J Hydrogen Energy 2007;32(13):2573–84.

[63] Mills RL, Sankar J, Voigt A, He J, Ray P, Dhandapani B. Role of atomic hydrogen density and energy in low power CVD synthesis of diamond films. Thin Solid Films 2005;478:77–90.

[64] Mills RL, Sankar J, Voigt A, He J, Dhandapani B. Spectroscopic characterization of the atomic hydrogen energies and densities and carbon species during helium-hydrogen-methane plasma CVD synthesis of diamond films. Chem Mater 2003;15:1313–21.

[65] Mills RL, Sankar J, Voigt A, He J, Dhandapani B. Synthesis of HDLC films from solid carbon," J. Materials science. J Mater Sci 2004;39:3309–18.

[66] Conrads H, Mills R, Wrubel Th. Emission in the deep vacuum ultraviolet from a plasma formed by incandescently heating hydrogen gas with trace amounts of potassium carbonate. Plasma Sources Sci Technol 2003;12:389–95.

[67] Mills RL, Onuma T, Lu Y. formation of a hydrogen plasma from an incandescently heated hydrogen-catalyst gas mixture with an anomalous afterglow duration. Int J Hydrogen Energy 2001;26(7):749–62. July.

[68] Mills RL. Temporal behavior of light-emission in the visible spectral range from a Ti-K_2CO_3-H-cell. Int J Hydrogen Energy 2001;26(No. 4):327–32.

[69] Mills R, Lotoski J, Kong J, Chu G, He J, Trevey J. High-power-density catalyst induced hydrino transition (CIHT) electrochemical cell. Int J Hydrogen Energy 2014;39:14512–30. https://doi.org/10.1016/j.ijhydene.2014.06.153.

[70] Mills RL, Dayalan E, Ray P, Dhandapani B, He J. Highly stable novel inorganic hydrides from aqueous electrolysis and plasma electrolysis. Electrochim Acta 2002;47(No. 24):3909–26.

[71] Reichhardt T. Out of this world. Nature 2002;420:10–1.

[72] Rathke A. A critical analysis of the hydrino model. New J Phys 2005;7:1–9. 127.

[73] Connett JE, Zimmerman PD. *Against hydrinos*, Phys. World 2005;18:21.

[74] Naudts J. On the hydrino state of the relativistic hydrogen atom. 2005, 0507193v2. arXiv:physics/.
[75] Rodgers P. Hydrogen results cause controversy. Phys World 2005;18:12–3.
[76] Dombey N. The hydrino and other unlikely states. Phys Lett A 2006;360:62–5.
[77] de Castro AS. *Orthogonality criterion for banishing hydrino states from standard quantum mechanics*. Phys Lett A 2007;369:380–3.
[78] Bourgoin RC. Inverse quantum mechanics of the hydrogen atom: a general solution. Adv Stud Theor Phys 2007;1:381–93.
[79] Guizzo E. Hot or not? IEEE Spectrum 2008;46:36–8.
[80] Phillips J. Selective atomic hydrogen heating in plasmas: implications for quantum theory. Int J Hydrogen Energy 2009;34:9816–23.
[81] Loureiro J, Amorim J. Possibility of nonexistence of hot and superhot hydrogen atoms in electrical discharges. Phys Rev E 2010;82:035401 (R).
[82] Phelps AV, Clementson J. Interpretation of EUV Emissions Observed by Mills et al. Eur J Phys D 2012;66:1–4. 120.
[83] Lawler JE, Goebel CJ. Comment on "time-resolved hydrino continuum Transitions with Cutoffs at 22.8 nm and 10.1 nm". Eur J Phys D 2012;66:1–2. 29.
[84] Selke DL. Against point charges. Appl Phys Res 2015;7:138–9.
[85] Poole HH. Atomic hydrogen III – the energy efficiency of atom production in a glow discharge. Proc. Roy. Soc. 1937;163:424–54.
[86] Ogita M, Saika N, Nkanishi Y, Hatanaka Y. Ga_2O_3 thin films for high-temperature gas sensors. Appl Surf Sci 1999;142:188–91.
[87] Trinchi A, Wlodarski W, Li YX. Hydrogen sensitive Ga_2O_3 Schottky diode sensor based on SiC. Sensor Actuator B 2004;100:94–8.
[88] Collins SE, Baltanás MA, Bonivardi AL. Hydrogen chemisorption on gallium oxide polymorphs. Langmuir 2005;21:962–70.
[89] Stoll S, Ozarowski A, Britt RD, Angerhofer A. Atomic hydrogen as high-precision field standard for high-field EPR. J Magn Reson 2010;207:158–63.
[90] Mitrikas G. Pulsed EPR characterization of encapsulated atomic hydrogen in octasilsesquioxane cages. Phys Chem Chem Phys 2012;14:3782–90.
[91] Li S-J, Zheng C, Lobring KC. Refinement of the crystal structure of gallium oxide hydroxide, Ga(O)OH. Kristallogr. NCS 2003;218:11–2.
[92] R.L. Mills, Parameters and magnetic energies due to the spin magnetic moment of H2(1/4), Ch. 16.7.5 (9 pages starting at equation 16.216) in Ref. 12.
[93] Portis AM. Electronic structure of F centers: saturation of the electron spin resonance. Phys. Rev. 1953;91:1071–8.
[94] Jones MT. Electron spin resonance absorption of tris-p-nitrophenylmethyl. J Chem Phys 1961;35:1146.
[95] Feldman VI, Sukhov FF, Orlov AY. Hydrogen atoms in solid xenon: trapping site structure, distribution, and stability as revealed by EPR studies in monoisotopic and isotopically enriched xenon matrices. J Chem Phys 2008;128:214511.
[96] Päch M, Stösser R. Scavenger assisted trapping of atomic hydrogen in Si_8O_{12} cages. J Phys Chem A 1997;101:8360–5.
[97] Beringer R, Castle JG. Microwave magnetic resonance spectrum of oxygen. Phys. Rev. 1951;81:82–8.
[98] McDonalds CC. Multiple-quantum transitions in EPR spectra of atomic oxygen. J Chem Phys 1963;39:3159–60.
[99] Hagen WR. Dislocation strain broadening as a source of anisotropic linewidth and asymmetric lineshape in the electron paramagnetic resonance spectrum of metalloproteins and related systems. J Magn Reson 1981;44:447–69.
[100] Hagen WR, Mills RL. Distinguishing electron paramagnetic resonance signature of molecular hydrino. 2020. https://assets.researchsquare.com/files/rs-144403/v1_stamped.pdf.